CNWRA ***A center of excellence in earth sciences and engineering***

A Division of Southwest Research Institute™
6220 Culebra Road • San Antonio, Texas, U.S.A. 78228-5166
(210) 522-5160 • Fax (210) 522-5155

November 26, 2001
Contract No. NRC–02–97–009
Account No. 20.01402.571

U.S. Nuclear Regulatory Commission
ATTN: Mrs. Deborah A. DeMarco
Two White Flint North
11545 Rockville Pike
Mail Stop T8 A23
Washington, DC 20555

Subject: Submittal of paper titled "Stress Corrosion Cracking of Nickel-Chromium-Molybdenum Alloys in Chloride Solutions" for the Annual NACE International Corrosion Conference and Exposition in Denver, Colorado, April 7–11, 2002

Dear Mrs. DeMarco:

Attached is the subject paper to be presented at the NACE International Corrosion Conference and Exposition to be held in Denver, Colorado, April 7–11, 2002. The paper describes the results of tests conducted to measure the stress corrosion cracking susceptibilities of Type 316L stainless steel and Alloy 22. The stress corrosion cracking susceptibility of Type 316 L stainless steel was found to be dependent on electrochemical conditions. The crack propagation rate was substantially reduced when the potential of the material was reduced below the repassivation potential for crevice corrosion. Alloy 22 was not found to be susceptible to stress corrosion cracking in concentrated chloride solutions. A portion of the information presented in this paper has been abstracted from Intermediate Milestone 1402.571.930 titled "Effects of Environmental Factors on the Aqueous Corrosion of High-Level Radioactive Waste Containers-Experimental Results and Models" which was previously reviewed and approved by U.S. Nuclear Regulatory Commission staff.

Please contact Darrell Dunn at 210.522.6090 if you have any questions regarding this paper.

Sincerely yours,

for

Budhi Sagar
Technical Director

BS:DD:jg
Attachment

cc:

J. Linehan	K. Stablein	T. Ahn	A. Henry	G. Cragnolino
B. Meehan	B. Leslie	C. Greene	W. Reamer	D. Dunn
E. Whitt	S. Wastler	J. Andersen	W. Patrick	Y.-M. Pan
J. Greeves	D. Brooks	J. Thomas	CNWRA Dirs	P. Maldonado
J. Piccone	T. McCartin	T. Essig	CNWRA EMs	T. Nagy (contracts)

Washington Office • Twinbrook Metro Plaza #210
12300 Twinbrook Parkway • Rockville, Maryland 20852-1606

STRESS CORROSION CRACKING OF NICKEL-CHROMIUM-MOLYBDENUM ALLOYS IN CHLORIDE SOLUTIONS

D.S. Dunn, Y.-M. Pan, and G.A. Cragnolino
Center for Nuclear Waste Regulatory Analyses
Southwest Research Institute
6220 Culebra Road
San Antonio, Texas 78238-5166

ABSTRACT

The stress corrosion cracking (SCC) susceptibilities of Alloy 22 and Type 316L stainless steel were evaluated in concentrated chloride solutions. Test results suggest that Alloy 22 is very resistant to chloride SCC. No SCC was observed after 12 months in 14.0 molal Cl^- as $MgCl_2$ at 110 °C using fatigue precracked wedge opening loaded double cantilever beam specimens with an initial stress intensity of 32.7 $MPa \cdot m^{1/2}$, however, minor grain boundary attack and limited secondary cracking were observed. Similar results were obtained in tests conducted using a stress intensity of 47 $MPa \cdot m^{1/2}$ with and without cyclic loading in 9.1 molal LiCl at 95 °C. The SCC susceptibility of Type 316L SS was sharply reduced when the potential of the material was reduced below the repassivation potential for crevice corrosion.

Keywords: Stress corrosion cracking, localized corrosion, stainless steel, nickel base alloys, nuclear waste disposal

INTRODUCTION

Stress corrosion cracking (SCC) of stainless steels and nickel base alloys has received much attention as a result of the wide spread use of these engineering alloys. The susceptibility of stainless steels and Ni base alloys to SCC has been examined by numerous investigators and extensively reviewed [1-5]. These investigations and reviews have demonstrated that SCC susceptibility is influenced by the alloy composition, impurities in the alloy, type and composition of aggressive species in the exposure environment, temperature, electrochemical conditions, stress, and distribution of flaws.

Many mechanisms have been proposed to predict SCC of engineering alloys [6]. While no one mechanism can satisfactorily explain the occurrence of SCC of multiple alloy systems [7], the slip dissolution mechanism seems to be the most appropriate for Ni-base alloys. In the slip dissolution model [8] stable anodic oxide film is fractured as a result of plastic deformation and anodic dissolution

of the metal occurs during repassivation. In addition, the lack of a SCC model that can be used to predict SCC susceptibility for a variety of alloys and systems, many SCC models have parameters that cannot be readily obtained [9]. Prediction of SCC susceptibility is necessary to assess the long term performance of engineered components such as containers for the geologic disposal of high level nuclear waste (HLW). In the absence of mechanistic models for SCC prediction, assessment of long term performance of engineered structures may be possible by bounding the SCC susceptibility of the alloy with respect to the range of expected exposure conditions.

Nickel base alloys are used in many applications in the chemical process industries as well as oil and gas production. The choice of Ni-base alloys in these applications is a result of the exceptional corrosion resistance of these materials in a wide variety of aggressive environments. The resistance of these alloys to SCC has been demonstrated to be strongly dependent on the chemical composition of the alloy [1,3,4]. SCC resistance in chloride solutions has been linked to the Ni content of the alloys. Copson [10] tested alloys with a range of Ni concentrations using wire specimens in boiling $MgCl_2$ and showed that the minimum resistence to SCC occurred when the Ni content of the alloy was approximately 12 percent. With either lower or higher Ni contents SCC failure times increased significantly and with very high Ni contents (>40 percent), SCC was not initiated. Subsequent work by Staehle et al. [1] with commercial Fe-Cr-Ni alloy wires using a constant strain technique, revealed that alloys with 50 percent Ni were not susceptible to SCC even in 45 percent $MgCl_2$ (15.7 molal Cl^-) at 154 °C. A large reduction in the SCC susceptibility was observed with alloys containing 30 percent Ni. Speidel [11] examined commercial alloys with 16 to 30 percent Cr, 1 to 73 percent Ni and 0 to 4.5 percent Mo in order to determine the response of these alloys using fracture mechanics type specimens in boiling 22 percent NaCl (105 °C). No SCC was observed for alloys with more than 40 percent Ni.

Studies conducted with susceptible alloys in aggressive environments have shown that the crack propagation rate and the initiation of stress corrosion cracking are dependent on electrochemical conditions [9]. Lee and Uhlig [12] observed an effect of potential on failure time by SCC using Ni and Ni 20 Cr alloys in $MgCl_2$ at 130 °C. When the applied potential was increased form –340 mV_{SCE} to –290 mV_{SCE}, the failure time decreased from 100 hours to 1 hour. Investigations by Silcock [13] using Type 316L stainless steel specimens in boiling 42 percent $MgCl_2$ (14.7 molal Cl^-) solutions at 154 °C showed a strong effect of potential on the SCC propagation rate. Higher stresses were needed to initiate SCC when the potential was sufficiently reduced. Russell and Tromans [14] tested cold worked type 316L SS T-double notch double cantilever beam specimens in $MgCl_2$ solutions at temperatures ranging from 116 to 154 °C and initial stress intensities, K_I, ranging from 12 to 100 $MPa{\cdot}m^{1/2}$. No SCC was observed on specimens with K_I in the range of 30 to 35 $MPa{\cdot}m^{1/2}$ in 44.7 percent $MgCl_2$ (15.6 molal Cl^-) at 154 °C when the potential was reduced below –0.350 V_{SCE}.

The SCC susceptibility of type 316 L stainless steel and Alloy 22 in concentrated chloride solutions are reported in this paper. Tests were conducted using fracture mechanics type specimens, such as wedge opening loaded double cantilever beam or compact tension specimens, in order to provide a preexisting flaw to facilitate the initiation of SCC [15]. Crack propagation rates were measured as a function of stress intensity and electrochemical conditions. The objectives of these investigations were to determine the SCC susceptibility of the alloys and measure the crack propagation rate as a function of exposure conditions; parameters that may be used to assess the performance waste packages for HLW disposal.

EXPERIMENTAL METHODS

The chemical compositions of the Alloy 22 and Type 316L heats used in this investigation are shown in Table 1. SCC tests were conducted using wedge opening loaded double cantilever beam specimens [16] (Figure 1) and compact tension fracture mechanics specimens (Figure 2) machined from hot-rolled and annealed plates. Specimens from 12.7-mm plate were machined with a long transverse-longitudinal direction (T-L) orientation where the crack plane is perpendicular to the width direction (T direction) and the crack propagation is in the longitudinal rolling direction (L direction). The 25.4-mm plate was used for the S-L orientation specimens where the fracture plane is perpendicular to the short transverse direction (S direction) and the crack propagation is in the L direction [17]. Test specimens were fatigue precracked using a servo hydraulic test machine. Specific conditions of precracking of each specimen was dependent on the test conditions. General guidelines for fatigue precracking specified in ASTM E399-90 Annex A2 [17] were adopted.

All SCC tests were conducted in 2-L test cells equipped with a fritted gas bubbler, platinum counter electrode, temperature probe, and a water cooled Luggin probe with a saturated calomel electrode (SCE) used as a reference maintained at room temperature. The SCC susceptibility was evaluated in concentrated $MgCl_2$ solutions (9.1 and 14.0 molal chloride) at 110 °C and concentrated LiCl (9.1 molal) solutions at 95 °C.

The double cantilever beam and compact tension specimens were periodically removed from the test cells and inspected with an optical microscope at low magnification. Scanning electron microscope (SEM) photographs were used to document the starting condition of the specimens and changes in surface features and/or signs of cracking. For the wedge opening loaded double cantilever beam specimens, the wedge was removed by loading the specimen in a servo-hydraulic load frame at the end of each test. A clip gage, installed to measure crack opening displacement, was used for the final compliance measurement. The final wedge load was also determined. The stress at which the crack is arrested, expressed in terms of the threshold stress intensity, K_{ISCC}, can then be calculated. At the completion of each test, the specimens were rinsed in deionized (DI) water and dried. Most specimens were cleaned ultrasonically in an inhibited hydrochloric acid (HCl) solution that contained 4 mL of 2-butyne-1,4-diol (35 percent aqueous solution), 3 mL of concentrated HCl and 50 mL of deionized water. Post-test examination was performed with an optical microscope and a SEM.

Double Cantilever Beam Specimens

For the double cantilever beam specimens the fatigue precracking was used to provide an initiation crack that extended past the specimen chevron notch. The SCC tests were conducted according to NACE Standard TM0177–96 [16]. Stress calculations were performed assuming that the double cantilever beam specimen was a straight beam subjected to pure bending. The bending stress of the double cantilever beam specimen arm at the crack tip can be calculated [18] according to Eq. (1)

$$\sigma = \frac{6Pa}{bh^2} \times 10^{-6} \tag{1}$$

where P is the wedge load, a is crack length, h is the height of the specimen arm, and b is specimen thickness. For σ in MPa, P is in Newtons, and a, b, and h are in meters.

The initial stress intensity, K_I, for the side grooved double cantilever beam specimen can be calculated [16,19] according to Eq. (2)

$$K_I = \frac{Pa(2\sqrt{3} + 2.38h/a)(b/b_n)^{1/\sqrt{3}}}{bh^{3/2}} \quad (2)$$

where b_n is the net thickness of the specimen at the side grooves in meters and K_I is in $Pa \cdot m^{1/2}$.

As reported previously by Pan et al.[20] the double cantilever beam specimens were fatigue-precracked under load control at 20 Hz, with a load ratio of 0.10 and a maximum stress intensity of 19.6 $MPa \cdot m^{1/2}$. Compliance curves were measured prior to wedge opening loading. The initial crack length for all specimens was approximately 32.8 mm. Alloy 22 double-tapered wedges were used to load the specimens to an initial stress intensity of 32.7 $MPa \cdot m^{1/2}$. The selection of the initial conditions was based on calculations of K_I and the double cantilever beam arm bending stress using Eq. (1). The yield strength of this heat of hot-rolled and mill-annealed Alloy 22 is 344 MPa. For a crack length of 32.8 mm, an initial loading of 2,482 N is required to achieve a K_I value of 34.8 $MPa \cdot m^{1/2}$. Under these loading conditions, the bending stress at the crack tip is 317 MPa, which is close to the yield strength of Alloy 22.

Compact Tension Specimens

SCC tests with compact tension specimens were conducted using both wedge opening loading and sustained loading conditions. The tests with wedge opening loading specimens are constant crack opening displacement tests in which the stress intensity decreases with crack growth, whereas in the constant load tests the stress intensity at increases as the crack propagates. Tests were also conducted using a cyclic loading with a frequency of 0.001 Hz and an R ratio of 0.7.

For all compact tension specimens a crack length/specimen width ratio, or a/W ratio, of 0.45 to 0.55 consistent with the ASTM E399 specifications [17] was used to determine the length of the initial fatigue precrack. In some cases, following the completion of fatigue precracking, specimens were wedge opening loaded using stress intensities below that used in the tests in order to allow the visual examination of the fatigue precrack with a microscope. After the fatigue precrack has been examined, the loading wedge was removed and the specimen was prepared for testing. For the wedge opening loading test specimens, tapered wedges were used to apply stress intensities at the specimen crack tip ranging from 21.8 to 54.5 $MPa \cdot m^{1/2}$. The stress intensity for the compact tension specimens in was calculated [21] according to Eq. (3)

$$K = \frac{f(a/W)P}{(BB_nW)^{1/2}} \quad (3)$$

where B is the specimen thickness, B_n is the thickness of the specimens at the side-grooves in meters and the function f(a/W) was calculated according to Eq. (4)

$$f(a/W) = \frac{\left(2+\frac{a}{w}\right)\left(0.886+4.64\frac{a}{W}-13.32\frac{a^2}{W^2}+14.72\frac{a^3}{W^3}-5.64\frac{a^4}{W^4}\right)}{\left(1-\frac{a}{W}\right)^{3/2}} \quad (4)$$

The limit load, P_L, for the compact tension specimens were determined [21] using Eq. (5)

$$P_L = c\eta B_e (W - a)\sigma_{YS} \quad (5)$$

where σ_{YS} is the yield strength of the material in MPa, c is a constant. B_e is the effective specimen thickness in meters and η is defined in Eq. (6)

$$\eta = \left[\left(\frac{2a}{b}\right)^2 + \left(\frac{4a}{b}\right) + 2\right]^{1/2} - \left[\frac{2a}{b}\right] - 1 \quad (6)$$

where b is the dimension of the uncracked ligament in meters determined by Eq. (7)

$$b = W - a \quad (7)$$

B_e is defined in Eq. (8)

$$B_e = \frac{(B - B_n)^2}{B} \quad (8)$$

For an a/W ratio of 0.45 the maximum stress intensity calculated using 80 percent of the P_L in Eq. (4) is 48 MPa·m$^{1/2}$ for Type 316L stainless steel (σ_{YS} = 276 MPa) and 61 MPa·m$^{1/2}$ for Alloy 22 (σ_{YS} = 345 MPa).

Testing of the statically loaded compact tension specimens was conducted in mechanical load frames using stress intensities from 20 to 47 MPa·m$^{1/2}$. Applied loads and specimen crack opening displacements were measured throughout the test. Specimen compliance was periodically measured by recording the crack opening displacement (COD) while slowly reducing the load and re-applying the load. The change in crack opening displacement (ΔCOD) was determined by subtracting the initial COD form the final COD at each time interval using Eq. (9)

$$\Delta COD = COD_{t=t} - COD_{t=0} \quad (9)$$

where $COD_{t=t}$ is the crack opening displacement at any time and $COD_{t=0}$ is the crack opening displacement immediately after the load was applied (time = 0). Tamaki et al. [22] showed that propagation of a crack through a Type 316 stainless steel tapered double cantilever beam specimen

resulted in measurable changes in compliance. Because the value of the compliance measurement obtained in this study were dependent on both the crack length and slight changes in the geometry of the load frame, a compliance ratio was used to compare time dependent changes in compliance measured in different tests. The compliance ratio was determined using Eq. (10)

$$\text{Compliance ratio} = \frac{\text{Compliance}_{t=t}}{\text{Compliance}_{t=0}} \tag{10}$$

where $\text{Compliance}_{t=t}$ is the compliance at any time during the test and $\text{Compliance}_{t=0}$ is the initial compliance measurement after the load was applied (time = 0). If stress corrosion cracking is initiated from the fatigue precrack and propagates through the specimen, the ΔCOD should increase from the initial value of 0 and the $\text{Compliance}_{t=t}$ should be greater than the $\text{Compliance}_{t=0}$ and the compliance ratio will be greater than 1. In the case where no stress corrosion cracking is initiated, the ΔCOD should remain at on near 0 and the compliance ratio should remain at or near 1 for the duration of the test. Finally, for the case where SCC is initiated and then stops, both the ΔCOD and the compliance ratio should increase while the crack is propagating and then remain constant after the crack is arrested.

RESULTS

Type 316 L stainless steel

The effect of potential on the SCC propagation rate for Type 316L stainless steel double cantilever beam and wedge opening loaded compact tension specimens tested with initial applied stress intensities of 22 to 33 $MPa\sqrt{m}$ is shown in figure 3. All tests were conducted using an initial stress intensity above the K_{ISCC} for type 316 L stainless steel that was determined to be 13.1 $MPa\sqrt{m}$ from wedge load measurements on double cantilever beam specimens exposed to 9.1 molal Cl^- as $MgCl_2$ [20]. The crack propagation rates were determined by measuring the length of the crack divided by the total test time [9, 20]. At potentials below the crevice corrosion repassivation potential (E_{rcrev}) measured to be in the range of –395 mV_{SCE} SCC was not observed even after 116 days of continuous exposure to concentrated chloride solutions. In contrast, SCC was quickly initiated when the potential of the specimen was maintained above the E_{rcrev}. The crack propagation rate was observed to be a dependent on potential. At –380 mV_{SCE} the crack propagation rate was in the range of 7.3×10^{-10} to 2.5×10^{-9} m/s. The crack propagation rate increased up to 1.8×10^{-8} m/s when specimens were tested at open circuit conditions where the corrosion potential (E_{corr}) was –330 to –320 mV_{SCE}.

Figure 4 shows results obtained with compact tension specimens tested under static loading conditions. All specimens were tested using an initial stress intensity of 47 $MPa\sqrt{m}$. It is apparent from figure 4 that significant COD and changes in compliance were observed for the specimen maintained at –350 mV_{SCE}. At the completion of the test, significant crack propagation was obvious and more than one crack was initiated. Examination of the fracture surface revealed transgranular crack growth that propagated a minimum of 4.4 mm from the end of the fatigue precrack. Assuming that cracking was initiated immediately after the load was applied the minimum crack growth rate is 6.5×10^{-9} m/s. No significant change in ΔCOD or compliance ratio was observed for specimens maintained at –375 and –400 mV_{SCE}. Both specimens showed some increase in the ΔCOD that is not

attributable to crack initiation and growth but mechanical deformation of the test specimen. It should be noted that the test at –375 mV_{SCE} was conducted in two test segments. The first test segment was approximately 300 hours and the second slightly under 900 hours. Because the compliance ratio is determined using the initial compliance at the start of the test, the compliance ratio at the start of the second test segment is 1.0. Although the compliance ratio appears to increase from the end of the first test segment to the start of the second test segment, this increase is a consequence of the method to determine the parameter plotted in figure 4 rather than an indication of SCC. For the specimen tested at –375 mV_{SCE}, it is apparent that the compliance ratio does not increase with time during the second test segment. For both specimens, the post test examinations revealed no indication of SCC.

The specimen tested at –400 mV_{SCE} was fractured by additional fatigue cycling in a servo hydraulic test machine. SEM micrographs of the fracture surface are included as figure 5. The fracture surface has two distinct regions, one associated with the initial fatigue precrack and the second associated with the fatigue after testing. Plastic deformation is visible between the fatigue regions. Detailed inspection of this region did not reveal any evidence of either interganular or transgranular SCC. The uncertainty in the SCC propagation is based on the resolution of the SEM inspection and the length of the test. Assuming a resolution of 10 microns and a test time of 839 hours, the uncertainty in the SCC propagation rate can be calculated to be 3.3×10^{-12} m/s.

The effect of stress intensity is shown in figure 6. When the stress intensity was reduced from 47 to 20 $MPa\cdot m^{1/2}$, the time for significant changes in ΔCOD and compliance ratio did not occur until after 700 hours of exposure. Post test examination of the specimen tested at 20 $MPa\cdot m^{1/2}$ revealed transgranular SCC (figure 7). The fracture surfaces of the two specimens were similar. It was not possible to determine when SCC was initiated in the test conducted at the lower stress intensity. Assuming that SCC was initiated immediately after the load was applied, reducing the stress intensity reduced the average crack propagation rate from 6.5×10^{-9} m/s to 2.3×10^{-9} m/s.

The effect of potential was also investigated using cyclic loading tests. Figure 8 shows the results obtained for a Type 316L SS specimens tested in 9.1 molal LiCl at –350 mV_{SCE} using cyclic loading for the first 30 hours of testing. After the first 30 hours a constant load was applied. The ΔCOD and the compliance ratio gradually increased for the first 100 hours of testing. A sharp increase in the compliance ratio was observed after 120 hours of testing indicating crack propagation. Examination of the specimen fracture surface revealed transgranular SCC (figure 9). An additional test was conducted in which the, the applied potential of the specimen was gradually decreased from –350 mV_{SCE} to –400 mV_{SCE} at a rate of 10 mV/hr after crack initiation and propagation (figure 10). Cyclic loading at a frequency of 0.001 Hz and an R ratio of 0.7 was continued as the potential was decreased. It is apparent from figure 10 that the ΔCOD increases during the first 250 hours of testing while the potential of the specimen was maintained at –350 mV_{SCE}. Once the potential was decreased the change in the ΔCOD slowed gradually. After changing from cyclic to static loading the ΔCOD increased abruptly several times before reaching a constant value after 500 hours. The lack of crack propagation is also indicated by the constant compliance ratio. The potential of the specimen was allowed to go to open circuit by disconnecting the potentstat. The E_{corr} in the air saturated solution is in the range of –340 to –350 mV_{SCE}. At open circuit, both the ΔCOD and the compliance ratio increased sharply indicating the re-initiation and propagation of cracks. Examination of the fracture surfaces following the test confirmed transgranular path.

Alloy 22

Tests were conducted [20] in 14.0 molal Cl^- as $MgCl_2$ with double cantilever beam specimens with a stress intensity of 32.7 $MPa\sqrt{m}^{1/2}$. After 21 weeks of exposure under open circuit conditions where the E_{corr} was in the range of –280 mV_{SCE} to –250 mV_{SCE}, grain boundary attack was observed on the side groove of a specimen with a T-L orientation, however, no SCC was identified on from either an initial inspection of the specimen side groove or a detailed examination of the fracture surface after the specimen was fractured by fatigue. Some minor cracking was observed on the side groove of a specimen with an S-L orientation after 10 weeks of testing. Continued exposure for a cumulative time of 52 weeks did not result in any crack propagation. At the end of the tests, the specimens were heat-tinted at 371 °C and then mechanically overloaded to failure. Examination of the fracture surfaces after testing clearly revealed both tinted and untinted regions on the fracture surface. No features consistent with SCC were observed, however, the appearance of the untinted region of the fracture surface, created as a consequence of mechanical overloading after exposure, tended to be flat and slightly faceted indicating a less ductile failure.

Results obtained with statically loaded Alloy 22 compact tension specimens using an initial stress intensity of 47 $MPa\sqrt{m}^{1/2}$ are shown in figure 11. The E_{rcrev} for Alloy 22 in this solution was measured to be –247 mV_{SCE} using cyclic polarization. Based on this measurement, the potential of the specimens were maintained close to the E_{rcrev} (–250 mV_{SCE}) and 5 to 30 mV above the E_{rcrev} (–245 mV_{SCE} to –220 mV_{SCE}). The specimens were exposed in 800 hour test segments at which time the specimens were removed from the test cell and examined for signs of SCC. At the start of the test, the ΔCOD increased to just greater than 0.1 mm for the specimen maintained above the E_{rcrev}. A smaller increase in the ΔCOD was observed for the specimen maintained close to the E_{rcrev}. After initially increasing, the ΔCOD remained constant for both specimens. A slight increase in the ΔCOD was observed at the start of each test segment. The compliance ratio was determined separately for each test segment. For both specimens, the compliance ratio was at or less than 1. The discontinuous increase in the compliance ratio from 0.98 to 1.00 for the specimen maintained anodic to the E_{rcrev} was a result of the re-initialization of the compliance ratio calculation rather than an indication of crack propagation. Visual examination of the side groove the specimens after exposure for 800 and 1600 hours revealed some plastic deformation that opened the crack and perhaps blunted the tip of the fatigue precrack. Some secondary cracking was observed on the specimens maintained anodic to the E_{rcrev}. The secondary cracks appeared to initiate at grain boundaries that were visible after fatigue precracking and prior to testing. This observation suggests that extensive mechanical damage and perhaps some intergranular fracture occurred during fatigue precracking. Testing of the specimens are continuing in order to assess the SCC resistance of Alloy 22.

A cyclic loading test of a fatigue precracked Alloy 22 compact tension specimen was also conducted in 9.1 molal LiCl (figure 12). The potential of the specimens was continuously maintained above the E_{rcrev}. An anodic current density of approximately 2×10^{-8} A/cm^2 was recorded when the applied potential was –230 mV_{SCE} or less. When the potential was increased to –225 mV_{SCE} a significant increase in the passive current was observed and the potential of the specimen was promptly reduced to avoid the initiation of localized corrosion. The ΔCOD and the compliance ratio were virtually constant over the entire test and were not influenced by variations in the applied potential. Examination of the sides of the specimens after testing revealed no indication of SCC. Additional exposures under similar conditions will be conducted.

DISCUSSION

Results obtained for Type 316L SS in concentrated chloride solutions show that SCC was rapidly initiated and crack propagation rates in the range of 10^{-9} to 10^{-8} m/s were measured [9, 20] when the potential of the test specimen was maintained above the E_{rcrev}. No SCC was initiated on specimens when the applied potential was maintained below the E_{rcrev}. Increasing the applied stress intensity at the crack tip from 22 to 54 MPa·$m^{1/2}$ did not increase the susceptibility of the material to SCC when the applied potential was less the E_{rcrev}. The effect of potential on the SCC susceptibility is in agreement with the results reported by Eremias and Marichev [23] who reported that in 10.8 molal LiCl solutions the K_{ISCC} for an austenitic stainless steel increased when the specimen potential was decreased.

Post-test examination of the compact tension specimen maintained below the E_{rcrev} revealed that the fracture surface was dominated ductile failure (figure 5). Linear features observed in figure 5 appear to be similar to cracks that are perpendicular to the fatigue precrack. Several investigations have reported crack branching in annealed stainless steels [24-26]. The features in figure 5 are not consistent with SCC. Dimples created by microvoid coalescence are visible over much of the area. These crack like features may be attributed to local ductile tearing as a consequence of the high stress intensity used in the test.

While the potentiostatic tests showed that SCC was not initiated as long as the potential of the test specimen was below the E_{rcrev}, it was desirable to determine the effect of potential on crack propagation. This was accomplished by conducting tests where SCC was initiated and allowed to propagate with the potential of the specimen above the E_{rcrev} prior to reducing the potential to just below the E_{rcrev}. The result shown in figure 10 suggests that the SCC propagation rate was substantially reduced when the potential of the specimen was lowering the potential of the specimen to a value a few mV less than the E_{rcrev}. The test was performed so that the potential of the specimen was gradually reduced in order to prevent sudden changes to the chemistry of the actively growing crack. Cyclic loading was continued for more than 30 hours after the potential of the specimen was reduced in order to promote SCC initiation and growth. After a static load was applied, the ΔCOD increased albeit slowly throughout the remaining duration of the test. The compliance ratio increased slightly for about 180 hours after the potential was reduced before eventually reaching a constant value. The plateau in the compliance ratio suggests that either the crack ceased to propagate or that the rate of crack propagation was slow and could not be detected by changes in compliance. It is not possible to conclusively state that the SCC was arrested when the potential of the specimen was reduced below the E_{rcrev} because there was a measurable increase in the COD as a function of time. It should be noted that the increase in the COD may not be an indication of SCC propagation. Because the combination of a constant load and an increase in the length of the crack as a consequence of SCC in the initial part of the test, the stress intensity at the crack tip also increased. Assuming that 80 percent of the crack propagation occurred in the initial 500 hours of the test (based on the observation that 80 percent of the ΔCOD occurred in the initial 500 hours of testing), the value of a/W would increase from 0.45 to 0.55. Correspondingly, the stress intensity at the crack tip would increase form 47 to 64 MPa·$m^{1/2}$. The increased stress intensity was in excess of the maximum stress intensity for plane stress conditions. Ductile yielding and ductile tearing, which are possible under these conditions, may be responsible for the increased COD while the potential was maintained at –400 mV_{SCE}.

Results obtained for Type 316L stainless steel in this study are partially in agreement with the previous results of Russell and Tromans [14] who reported the arrest of SCC for 316L in 44.7 percent $MgCl_2$ (15.6 molal chloride) when the potential was reduced from –250 mV_{SCE} to –350 mV_{SCE}. Crack

arrest was not instantaneous, however, and was reported to gradually decrease over a period of 5,500 seconds. In addition, the minimum crack propagation rate reported by after SCC arrest was 10^{-9} m/s which was substantially lower than the crack propagation rates of 4×10^{-7} m/s at higher potentials. The differences in crack propagation rates measured by Russell and Tromans [14] and those measured in this study can be attributed to differences in the type of test specimens and testing conditions. Both testing time and the resolution of the crack growth rate were not reported in the work of Russell and Tromans [14]. As a result, it is not possible to determine if SCC arrest was achieved by reducing the potential, or if the rate of SCC propagation continued at a rate less than 10^{-9} m/s. The results of tests performed in this study suggest that the SCC propagation rate is reduced when the potential was reduced below the E_{rcrev}. However, a conclusive determination of crack arrest may only be possible using lower stress intensities where ductile failure is not a concern.

Tests conducted with Alloy 22 do not conclusively indicate this material is susceptible to SCC in concentrated chloride solutions. The absence of SCC under the conditions investigated are in agreement with the original results reported by Copson [10] that alloys with more than 40 percent Ni are resistant to chloride SCC. In later work by Speidel [11] using fracture mechanics type specimens with an initial stress intensity of 60 $MPa\cdot m^{1/2}$, no SCC was initiated on alloys containing more than 40 percent Ni in boiling concentrated NaCl solutions. In this investigation, limited secondary cracking and increased COD obtained under constant loading conditions when the potential was maintained above the E_{rcrev} suggest that chloride SCC may be possible under very aggressive conditions; however the SCC propagation rate may be very slow. In addition the potential range for SCC decreases as the chloride concentration increases. The previous work of Tamaki et al. [22] suggests that in concentrated chloride solutions, the potential range for SCC may be limited to a few mV greater than the E_{rcrev}. At higher potentials, localized corrosion in the form of crevice corrosion may occur preferentially to SCC. The significant increase in current observed when the potential of the Alloy 22 specimen was increased to -225 mV_{SCE} and the visual confirmation of crevice corrosion are consistent with the observations of Tamaki et al. [22]. An attempt to use cyclic loading to initiate SCC was based on the recently reported results of Andresen et al. [27]. Using cyclic loading at a frequency of 0.001 to 0.003 Hz Andresen et al. [27] reported the initiation of SCC on Alloy 22 in concentrated high pH salts solutions at 110 °C. The crack growth rates reported by Andresen et al. [27] are on the order of 5×10^{-13} m/s. At this low crack propagation rate, test times of more than 200 days are needed to have a crack extension of 0.01 mm.

CONCLUSIONS

The susceptibility of Alloy 22 and Type 316L stainless steel was investigated in concentrated chloride solutions. Type 316 L stainless steel was found to be susceptible to SCC when the potential of the specimen was above the E_{rcrev}. In contrast, the initiation of SCC was prevented when the potential is less than the E_{rcrev}. When the potential of the specimen was reduced below the E_{rcrev} after crack initiation and propagation, the SCC propagation rate was substantially reduced as implied by changes in the COD and compliance. However, it is not possible to conclude that SCC is arrested when the specimen potential is reduced below the E_{rcrev} Additional tests are planned to better assess the effect of potential on the SCC propagation rate.

Alloy 22 was found to be very resistant to SCC in concentrated chloride solutions. No conclusive determination of Alloy 22 SCC susceptibility could be made from the results of the tests

conducted in this investigation. Additional tests in progress will help to establish the relationship between the E_{rcrev} and the SCC susceptibility of Alloy 22.

ACKNOWLEDGEMENTS

This paper was prepared to document work preformed by the CNWRA for the NRC under Contract No. NRC–02–97–009. The activities reported here were performed on behalf of the NRC Office of Nuclear Material Safety and Safeguards, Division of Waste Management. The paper is an independent product of the CNWRA and does not necessarily reflect the views or the regulatory position of the NRC.

REFERENCES

1. R.W. Staehle, J. J. Royuela, T. L. Raredon, E. Serrate, C. R. Morin, and R. V. Farrar, Corrosion 26, 11(1970): 451-486.

2. G.J. Theus, and R.W. Staehle, "Review of stress corrosion cracking and hydrogen embrittlement in the austenitic Fe-Cr-Ni alloys, " Stress Corrosion Cracking and Hydrogen Embrittlement of Iron Base Alloys, NACE-5, R. W. Staehle, J. Hochmann, R. D. McCright, and J. E. Slater eds. (Houston, TX: National Association of Corrosion Engineers, 1977): 845-892.

3. R.H. Jones, and S. M. Bruemmer, "Environment-induced crack growth processes in nickel-base alloys. In Environment-Induced Cracking of Metals," NACE-10, R. P. Gangloff and M. B. Ives eds. (Houston, TX: National Association of Corrosion Engineers 1990): 287-310.

4. N. Sridhar, and G. A. Cragnolino, "Stress-corrosion cracking of nickel-base alloys," Stress Corrosion Cracking - Materials Performance and Evaluation, R.H. Jones, ed. (Materials Park, OH: ASM International 1992): 131-179.

5. A.J. Sedricks, "Stress-Corrosion Cracking of Stainless Steels," Stress Corrosion Cracking - Materials Performance and Evaluation, R.H. Jones, ed. (Materials Park, OH: ASM International 1992): 91-130.

6. R.H Jones, and R.E. Ricker, "Mechanisms of Stress-Corrosion Cracking," Stress Corrosion Cracking - Materials Performance and Evaluation, R.H. Jones, ed. (Materials Park, OH: ASM International 1992): 1-40.

7. N. Sridhar, J.C. Walton, G.A. Cragnolino, and P.K. Nair. "Engineered barrier system performance assessment codes (EBSPAC) Progress Report - October 1, 1992, through September 25, 1993," Center for Nuclear Waste Regulatory Analyses, CNWRA 93-021, 1993.

8. G. Cragnolino, and D.D. Macdonald. 1982. Corrosion 38,8(1982): 406-424.

9. G.A. Cragnolino, D.S. Dunn, Y.-M. Pan, and N. Sridhar. "The Critical Potential for the Stress Corrosion Cracking of Fe-Cr-Ni Alloys and Its Mechanistic Implications," Chemistry and Electrochemistry of corrosion and Stress Corrosion Cracking: A Symposium Honoring the

Contributions of R.W. Staehle. R.H. Jones ed, (Warrendale, PA: The Minerals, Metals and Materials Society, 2001): pp. 83-104.

10. H.R. Copson, "Effect of composition on stress corrosion cracking of some alloys containing nickel," Physical Metallurgy of Stress Corrosion Cracking, T.N. Rhodin, ed. (New York, NY Interscience Publishers,1959): 247-269.

11. M.O. Speidel, Metallurgical Transactions, 12A(1981):779-789.

12. H.H. Lee and H.H Uhlig, Journal of the Electrochemical Society, 117,1(1970): 18-22.

13. J.M. Silcock, Corrosion 38,3(1982): 144-156.

14. A.J. Russell, and D. Tromans. Metallurgical Transactions 10A(1979): 1229-1238.

15. J. Kruger, "Mechanisms and applications of nickel base alloys," Corrosion of Nickel-Base Alloys. (American Society for Metals,1985):1-11.

16. NACE International. *Testing of Metals for Resistance to Sulfide Stress Cracking at Ambient Temperatures.* NACE Standard TM0177–96. Houston, TX: NACE International. 1996.

17. American Society for Testing and Materials. Standard test method for plane-strain fracture toughness of metallic materials: E399–90. Annual Book of ASTM Standards. Volume 03.01: Metallography. Metals—Mechanical Testing: Elevated and Low-Temperature Tests, (West Conshohocken, PA: American Society for Testing and Materials, 1999): 422–452.

18. S. H. Crandall, N.C. Dahl, and T.J. Lardner, An Introduction to the Mechanics of Solids, 3rd Edition, New York: McGraw-Hill, Inc. 1978.

19. R.B. Heady, Corrosion 33,7(1977): 98–107.

20. Y.-M. Pan, D. S. Dunn, and G. A. Cragnolino, "Effects of Environmental Factors and Potential on Stress Corrosion Cracking of Fe-Ni-Cr-Mo Alloys in Chloride Solutions," Environmentally Assisted Cracking: Predictive Methods for Risk Assessment and Evaluation of Materials, Equipment, and Structures. STP 1401. R. D. Kane ed. (West Conshohocken, PA: American Society for Testing and Materials, 2000): 273-288.

21. T.L. Anderson, Fracture mechanics - Fundamentals and Applications, (Boca Raton, FL: CRC Press, 1991) 716-717.

22. K. Tamaki, S. Tsujikawa, and Y. Hisamatsu, Advances in Localized Corrosion. H.S. Isaacs, U. Bertocci, J. Kruger, and S. Smialowska, eds. (Houston, TX: National Association of Corrosion Engineers, 1990): 207–214.

23. B. Eremias, and V.V. Marichev, Corrosion Science 20(1980): 307–312.

24. M.O. Speidel, Corrosion 32(1976): 187-190.

25. M.O. Speidel, Corrosion 33(1977): 199-203

26. R.W. Staehle, Theory of Stress Corrosion Cracking in Alloys, J.C. Scully, ed. (Brussels: North Atlantic Treaty Organization, 1971): 223–288.

27. P.L. Andresen, P.W. Emigh, L.M. Young, and G.M. Gordon, "Stress Corrosion cracking of annealed and cold worked titanium grade 7 and Alloy 22 in 110 °C concentrated salt environments," CORROSION/2001 paper no. 130. (Houston, TX: NACE International, 2001).

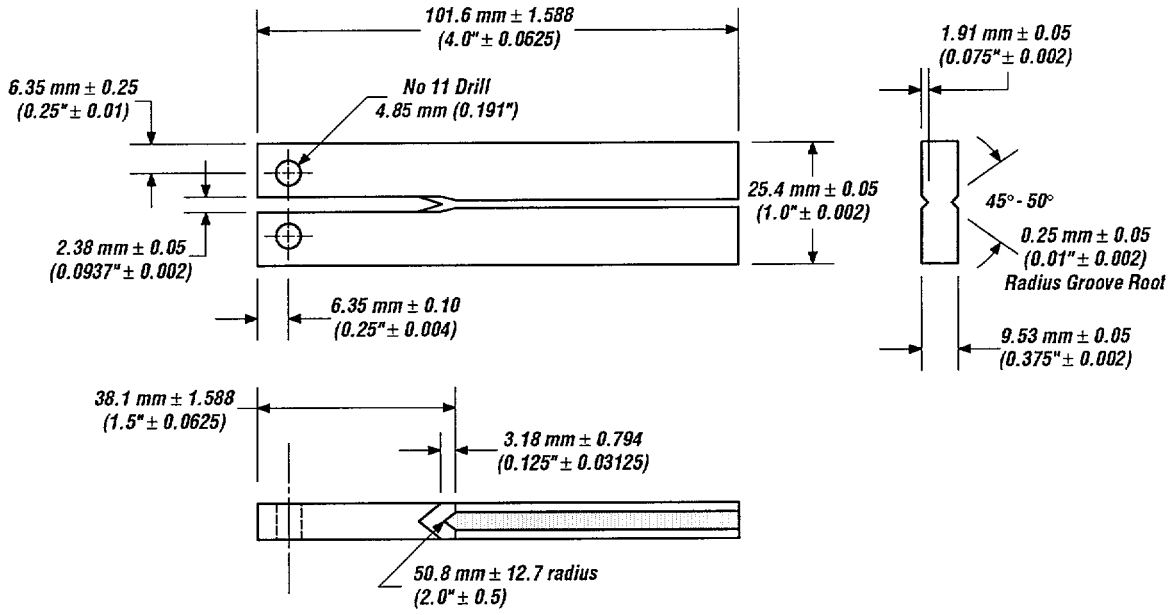

Figure 1. Dimensions of the double cantilever beam specimens according to NACE TM0177-96.

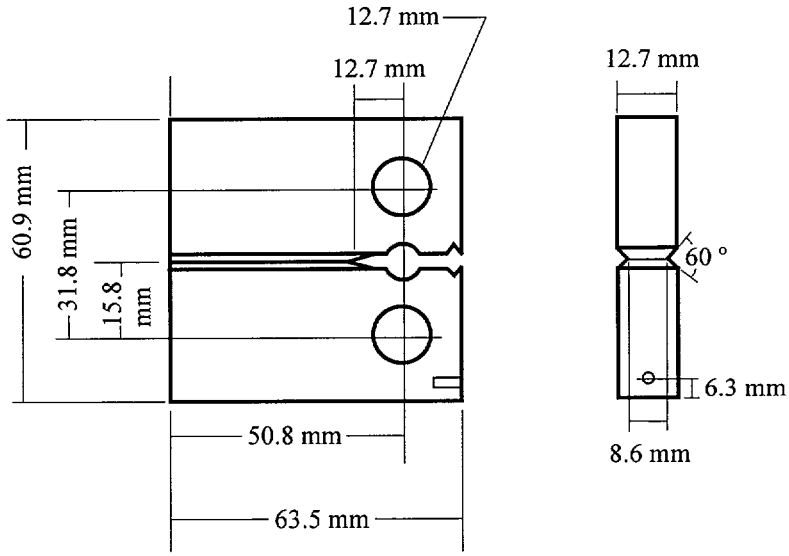

Figure 2. Dimensions of the compact tension specimens

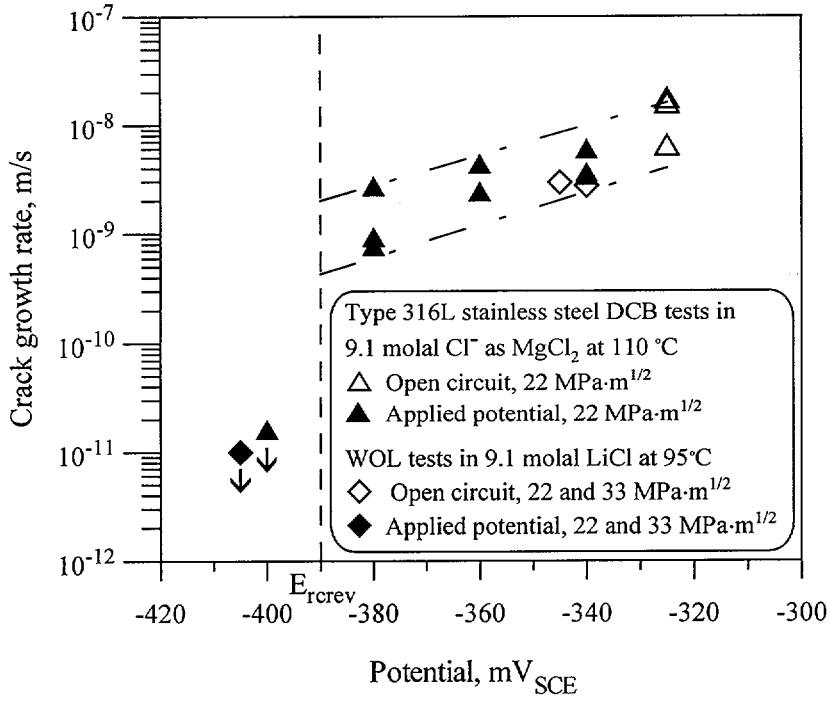

Figure 3. Crack growth rate for type 316L stainless steel as a function of potential in concentrated chloride solutions

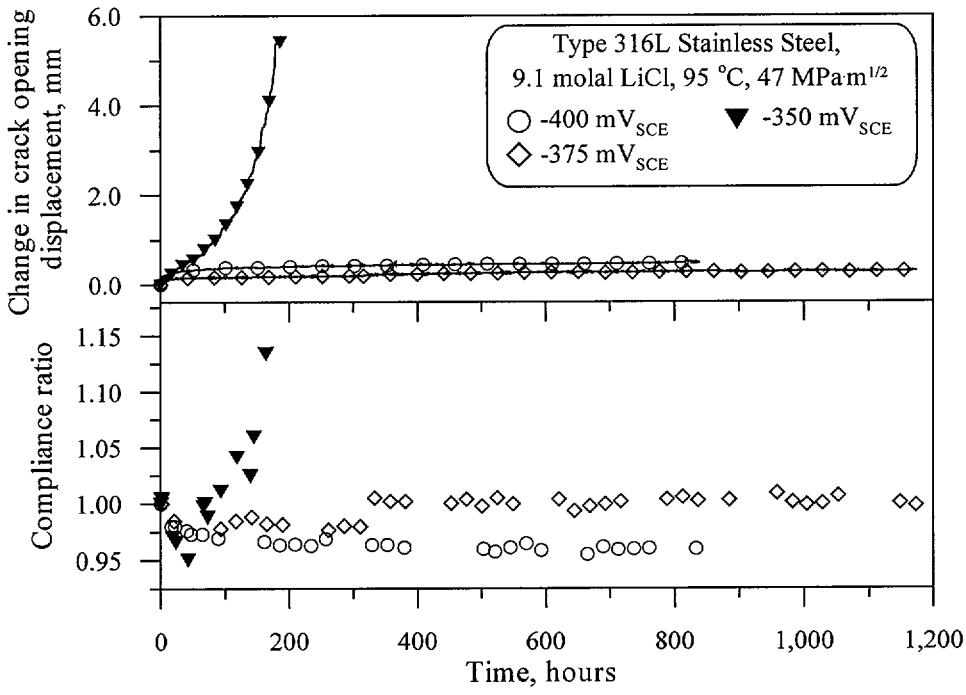

Figure 4. Change in crack opening displacement and compliance ratio as a function of potential for type 316L stainless steel compact tension specimens tested in 9.1 molal LiCl

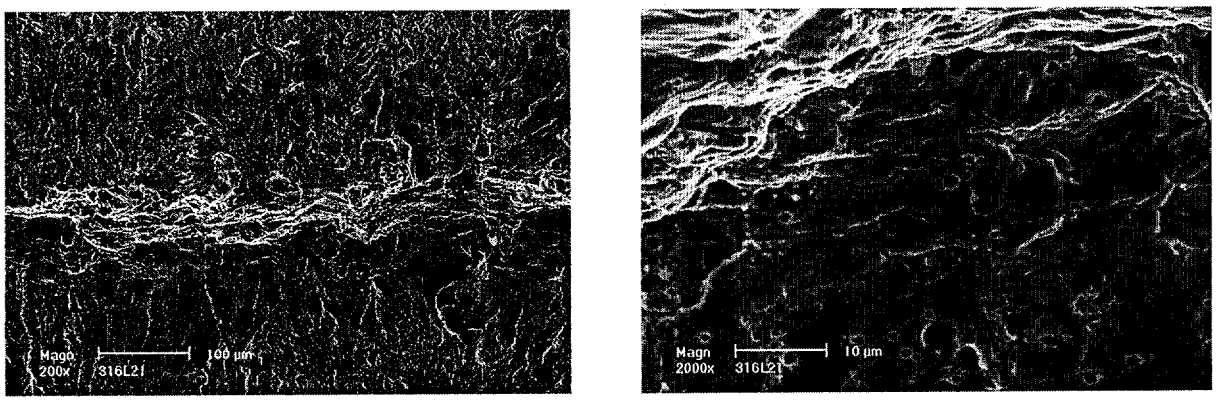

Figure 5. Scanning electron micrographs of fracture surface of type 316L stainless steel after testing at –400 mV_{SCE} in 9.1 molal LiCl. The initial stress intensity was 47 $MPa\cdot m^{1/2}$

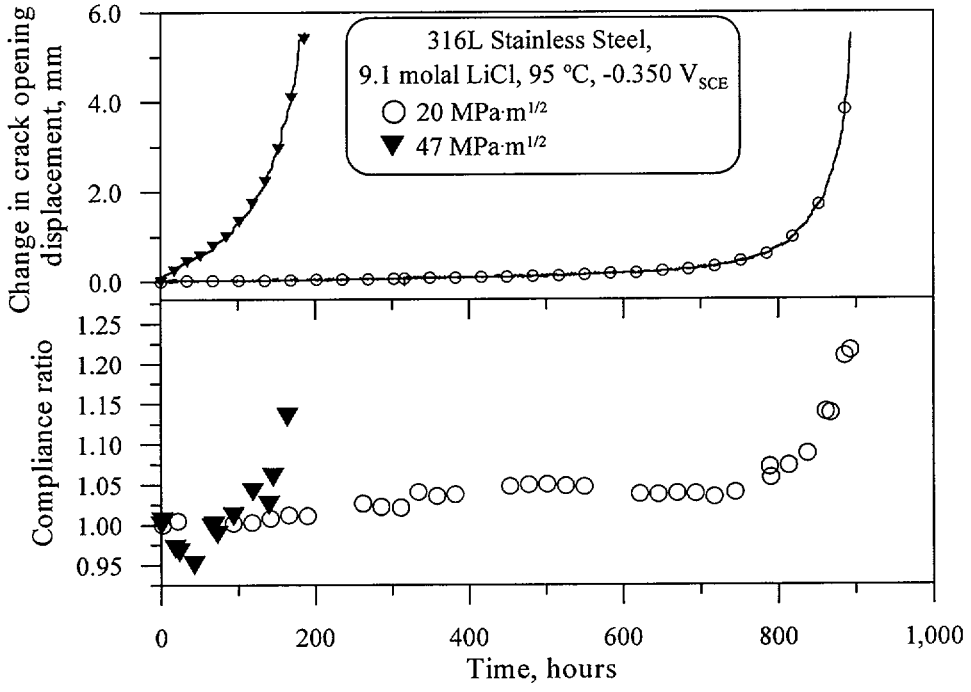

Figure 6. Change in crack opening displacement and compliance ratio as a function of initial stress intensity for type 316L stainless steel compact tension specimens tested in 9.1 molal LiCl at a potential of –350 mV_{SCE}

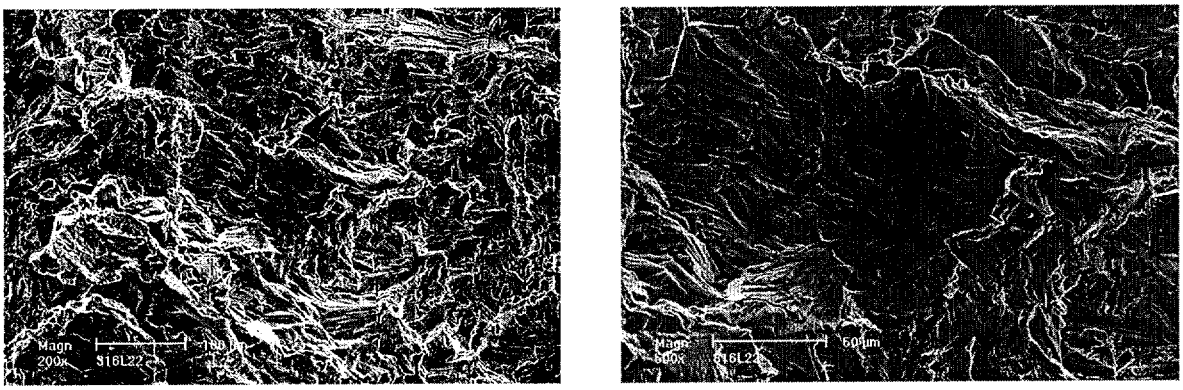

Figure 7. Scanning electron micrographs of fracture surface of type 316L stainless steel after testing at –350 mV_{SCE} in 9.1 molal LiCl. The initial stress intensity was 20 $MPa\cdot m^{1/2}$.

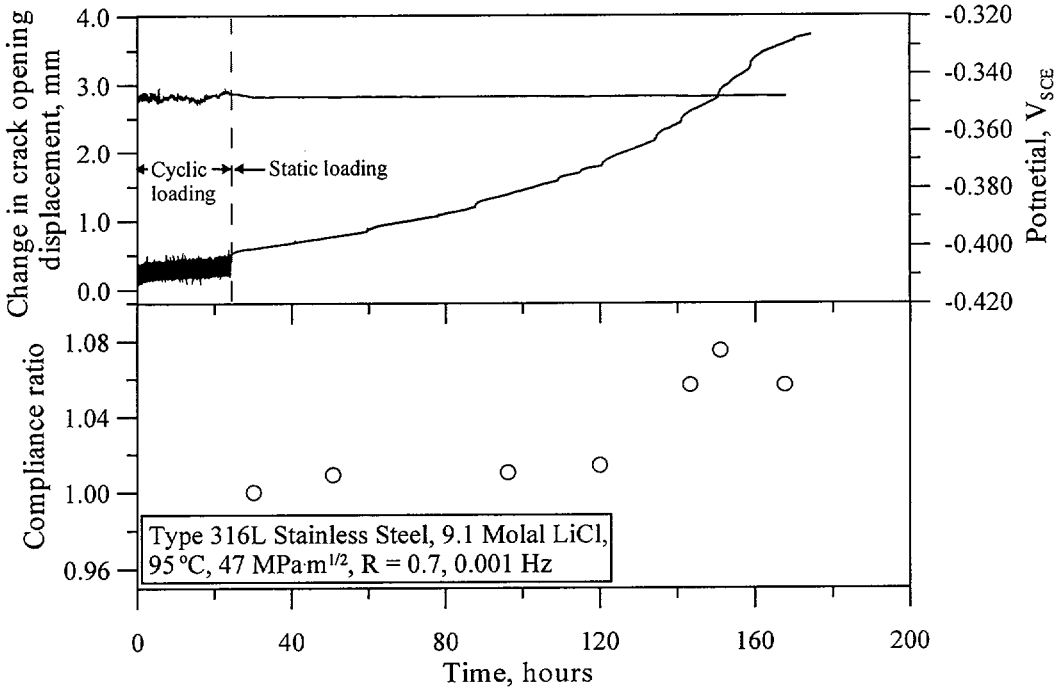

Figure 8. Change in crack opening displacement and compliance ratio for a type 316L stainless steel compact tension specimen tested in 9.1 molal LiCl at a potential of –350 mV_{SCE}. Cyclic loading was used to initiate stress corrosion cracking.

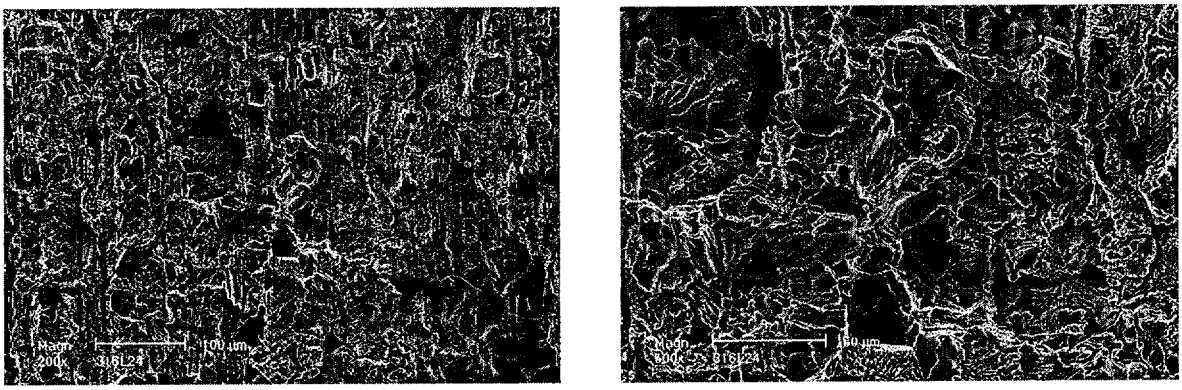

Figure 9. Scanning electron micrographs of fracture surface of type 316L stainless steel after testing at –350 mV_{SCE} in 9.1 molal LiCl. The initial stress intensity was 47 $MPa\cdot m^{1/2}$. Cyclic loading at 0.001 Hz with R = 0.7 was used to initiate stress corrosion cracking

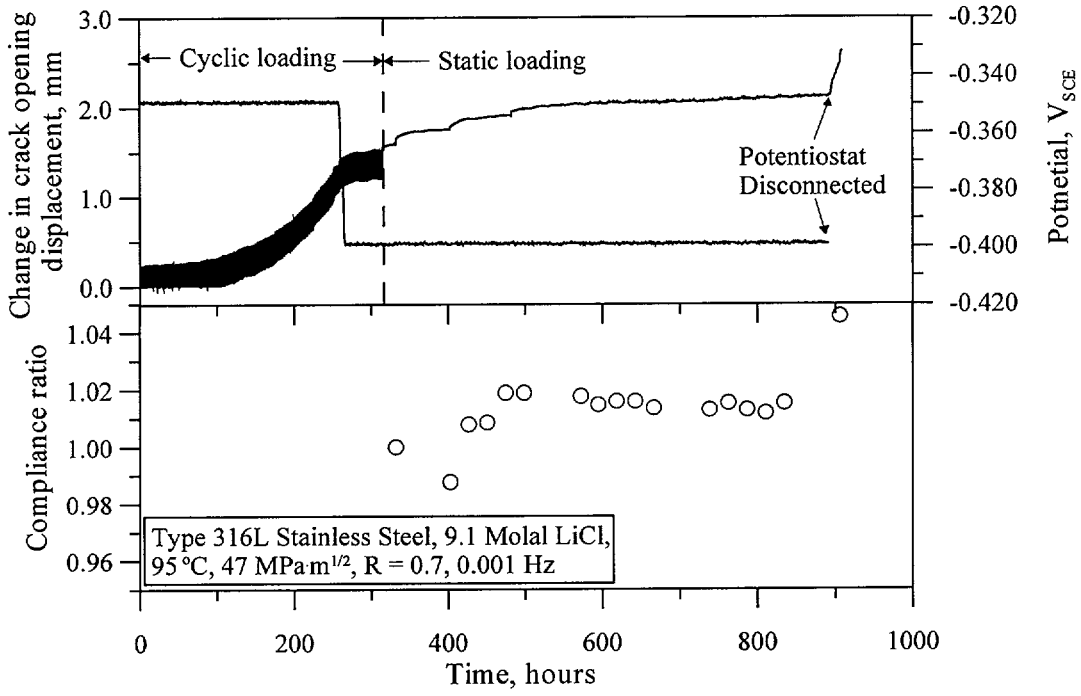

Figure 10. Change in crack opening displacement and compliance ratio for a type 316L stainless steel compact tension specimen tested in 9.1 molal LiCl. Cyclic loading at a potential of –350 mV_{SCE} was used to initiate stress corrosion cracking.

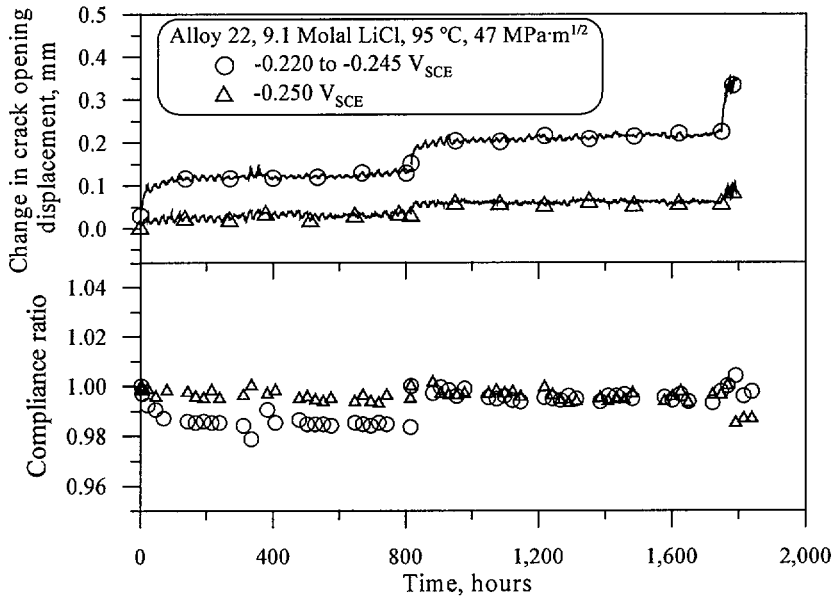

Figure 11. Change in crack opening displacement and compliance ratio for Alloy 22 compact tension specimens tested in 9.1 molal LiCl.

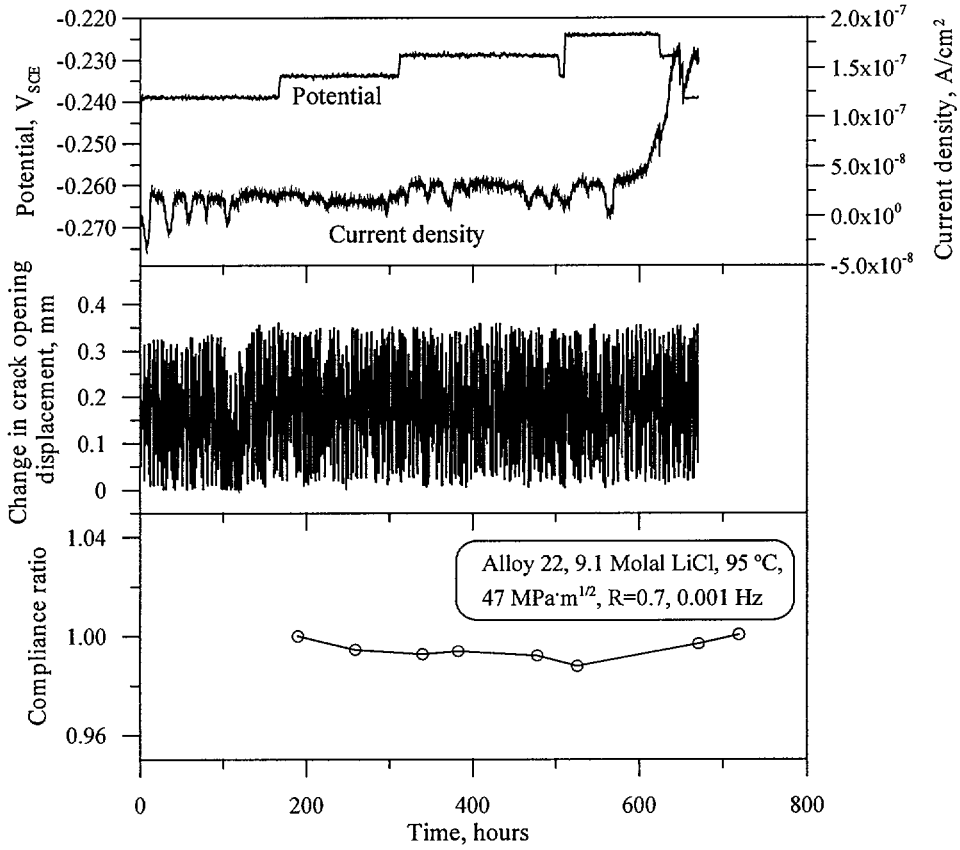

Figure 12. Change in crack opening displacement and compliance ratio for Alloy 22 compact tension specimens tested in 9.1 molal LiCl under cyclic loading conditions